International Journal of Mass Spectrometry
May 2016, Volume 402, Pages 20-28
http://dx.doi.org/10.1016/j.ijms.2016.02.013
http://archimer.ifremer.fr/doc/00317/42863/

Differentiation of gonyautoxins by ion mobility - mass spectrometry; a cationization study

Poyer Salomé [1], Loutelier-Bourhis Corinne [1], Tognetti Vincent [1], Joubert Laurent [1], Enche Julien [1], Bossée Anne [3], Mondeguer Florence [2], Hess Philipp [2], Afonso Carlos [1, *]

[1] Normandie Université, COBRA, UMR 6014 et FR 3038; Université de Rouen; INSA de Rouen; CNRS, IRCOF, 1 rue Tesnière, 76821 Mont Saint Aignan Cedex, France
[2] IFREMER, Laboratoire Phycotoxines, F-44311 Nantes 03, France
[3] DGA Maîtrise NRBC, département Analyse Chimique, F-91710 Vert Le Petit, France

* Corresponding author : Carlos Afonso, Tel.: +33 235522940. ;
email address : carlos.afonso@univ-rouen.fr

Abstract :

Gonyautoxins are potent natural neurotoxic analogues of saxitoxin. Due to their biological activity and submilligram lethal dose for man, fast and efficient methods are required for their characterization. Recent advances in ion mobility-mass spectrometry (IM-MS) showed that differentiation of isomers could be achieved using specific experimental conditions involving particular buffer gases as well as cationic species. In this work, IM-MS experiments were carried out using alkali metal ions (Met = Li+, Na+ or K+) and different buffer gases (N2, N2O and CO2) to improve the differentiation of gonyautoxin isomers. The separation of [GTX + Met]+ ion was achieved for GTX2/3 and GTX1/4 from their Na or K adducts. For dcGTX2/3, the ion mobility separation can only be obtained with peak to peak resolution (Rp-p) close to 1 from the [GTXs + Met − H2O]+ species. To understand the gas phase conformation of the different diastereomers, density functional theory (DFT) calculations were performed. IM separation, and collision cross sections on [GTXs + Met]+ and [GTXs + Met − H2O]+ are reported for the first time.

Graphical abstract

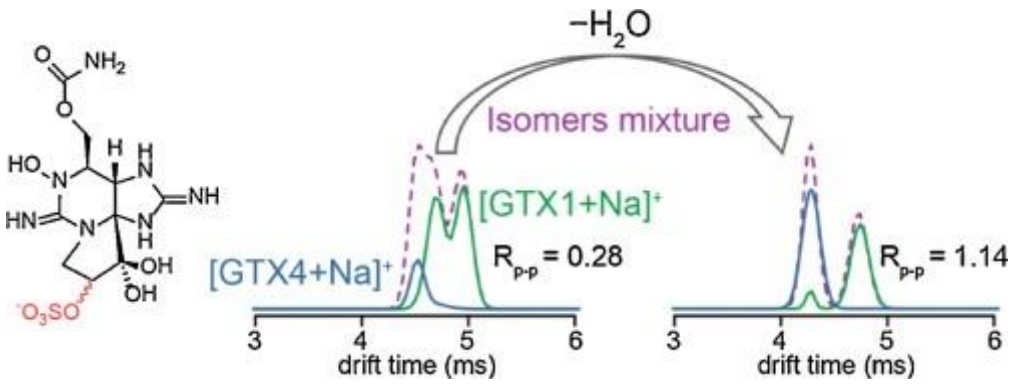

Highlights

► Ion mobility separation of gonyautoxin isomers is achieved using cationized species. ► Experimental and theoretical collision cross-sections of alkali gonyautoxins are determined. ► Loss of water from cationized gonyautoxins improves ion mobility separation.

Keywords : ion mobility, gonyautoxin, collision cross section, alkali adduct

INTRODUCTION

Gonyautoxins (GTXs) are analogues of saxitoxins (STXs), a group of toxins that generate the paralytic shellfish poisoning syndrome by binding to voltage-gated sodium and potassium channels sites [1, 2]. Saxitoxin is listed in the schedule 1 of the Chemical Weapon Convention because of their potential historical use in darts (TZ agent), their toxicity and also the possibility to produce them in large scale by organic synthesis or culture of micro-organisms [3, 4]. Gonyautoxins are principally produced by dinoflagellates in marine water (*Gymnodinium* and *Alexandrium*) and cyanobacteria in freshwater (*Anabaena circinalis, Aphanizomenon spp., Lyngyba wollei*) [5, 6]. The different gonyautoxins present similar toxicities, but they show higher LD_{50} than the saxitoxin for which a submilligram dose is lethal to man [7, 8]. The identification of GTX analogues represents a significant analytical challenge, due to the presence of numerous isomers and their very high polarity (Table 1).

Table 1. Structure of gonyautoxins studied in the present work and corresponding stereochemistry.

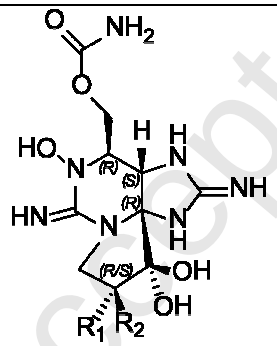
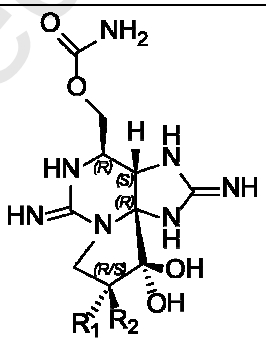
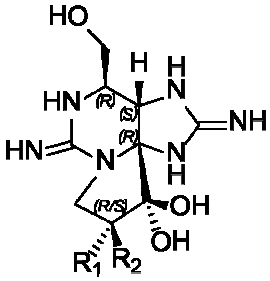

Stereo	Toxin	R_1	R_2	Toxin	R_1	R_2	Toxin	R_1	R_2
R,S,R,S	GTX4	H	OSO_3^-	GTX3	H	OSO_3^-	dcGTX3	H	OSO_3^-
R,S,R,R	GTX1	OSO_3^-	H	GTX2	OSO_3^-	H	dcGTX2	OSO_3^-	H

The separation and identification of GTXs have previously been reported using various analytical methodologies; liquid chromatography with pre- or post- column oxidation and fluorescence detection [9, 10], hydrophilic interaction liquid chromatography-mass spectrometry (HILIC-MS) [11], LC-MS [12], isotachophoresis/capillary electrophoresis [13],

and more recently, HILIC coupled to ion mobility - mass spectrometry (HILIC-IM-MS) [14, 15]. All these approaches involved chromatographic separation and were therefore time-consuming. There are obvious advantages in the development of faster analytical methods for detection and identification of GTX using commercially available instruments.

IM is a separation method based on the size, shape and charge of ions in gas phase and appears to be a technique of choice for the fast identification of isomers when coupled to mass spectrometry [16-18]. One obvious advantage of IM is the speed of the analysis as typical ion mobility spectra are recorded in less than 100 ms. Recent studies showed a larger range of applications using specific drift gases such as CO_2 and N_2O rather than N_2 and He that are commonly used [19, 20]. Indeed, depending on its polarizability, the gas can change the ion separation and can improve, in some cases, the separation of isomers. On the other hand, cationization is known to (i) form ions that are more stable in the gas phase than protonated molecules and (ii) increase collision cross section (CCS) difference between isomer adducts [16, 21, 22]. The formation of alkali adducts of GTXs were examined as their gas phase stability could avoid the fragmentation of the ion usually encountered for protonated GTXs in the positive ionization mode. Indeed, previous studies reported that the protonated forms of GTX1, GTX2 and dcGTX2 easily dissociate yielding abundant $[GTX+H-SO_3]^+$ fragment ions [11, 23].

The aim of this work is to evaluate the capability of IM-MS for fast analysis of GTXs without upstream LC separation. Different alkali adducts (Met) as well as different IM gases were studied to improve the differentiation of GTX isomers. Both $[GTXs+Met]^+$ and $[GTXs+Met-H_2O]^+$ species were investigated in order to separate the three isomer couples usually observed in algae and mollusks, namely GTX1/4, GTX2/3 and dcGTX2/3. CCS values were determined and compared to theoretical structures to understand the gas phase behavior of GTX analogues.

EXPERIMENTAL

Chemicals and standard solutions

Certified standards of GTXs (GTX1/4 75/25 mmol L^{-1}, dcGTX2/3 82/18 mmol L^{-1}, and GTX2/3 72/28 mmol L^{-1}) were purchased from the National Research Council Canada. HPLC-grade acetonitrile (MeCN) was supplied by VWR (Fontenay-sous-Bois, France), polyalanine, formic acid 99 and sodium chloride (NaCl), from Sigma-Aldrich (Saint Quentin-Fallavier, France). Deionized water (18.2 MΩ) was obtained from a Milli-Q apparatus (Waters, Saint-Quentin-Yvelines, France). Lithium iodide (LiI) and potassium iodide (KI) were purchased from Strem Chemicals (Newburyport, U.S.A.). N_2O-N40, CO_2-N48 and N_2-N47 ion mobility gases were purchased from Air Liquide (France).

HILIC conditions

HILIC separation was performed using an ultra-high performance liquid chromatography (Nano Acquity, Waters, Manchester, UK) system equipped with binary pumps, degasser, thermostated autosampler and column heater maintained at 5°C and 45°C respectively. The system was fitted with a BEH amide column (1.7 µm, 1 mm x 150 mm) manufactured by Waters (San Francisco, CA, USA). Eluent A was a mixture of 2 mmol L^{-1} ammonium formate buffer with either 1 mmol L^{-1} of LiI, 2 mmol L^{-1} of NaCl or 1 mmol L^{-1} of KI, adjusted to pH 3.5 with formic acid and B was acetonitrile containing 5% of eluent A. The elution gradient was as following: 0 min (80% B), 4 min (55% B), 8 min (55% B), 10 min (25% B), 13 min (25% B) and 16 min (80% B). An equilibration time of 4 min was required for this column to return to initial conditions for a total run time of 20 min. A flow rate of 80 µL min^{-1} and a sample volume injection of 1 µL were used. Commercial toxin solutions were directly injected and GTX mixture was diluted to 3 mg L^{-1} in H_2O/MeCN 50:50 (v/v).

Masslynx v4.1 and Driftscope v2.2 software were used to process data (Waters, Manchester, UK).

IM-MS conditions

Ion mobility - mass spectrometry experiments were carried out using a hybrid quadrupole-ion mobility-time-of-flight mass spectrometer (Synapt G2 HDMS, Waters, Manchester, UK) largely described [24-26]. The ESI source was operated in the positive and the negative ionization modes due to the zwitterionic feature of GTXs derivatives. The source temperature was set to 70°C, the desolvation gas (N_2) temperature at 250°C and the gas flow to 500 L hr^{-1}. Voltage parameters for the positive ionization mode were the following: capillary 3 kV, sampling cone 30 V, extraction cone 5 V, cone gas flow 20 L hr^{-1}. In-source CID (collision Induced Dissociation) experiments were performed after tuning source voltages, temperatures and gas flow with infused solutions. The optimized conditions for in-source CID were: capillary voltage 4.0 kV, sampling cone 55.0 V, extraction cone 5.0 V, source temperature 90°C, desolvation temperature 350°C, desolvation gas flow 500 L hr^{-1} and cone gas flow 300 L hr^{-1}.

For IM experiments, data were acquired using 300 µs of mobility delay after trap release. The helium cell gas flow was set to 180 mL min^{-1} and IM gas flow, wave height and velocity were dependent of the IM gas, and adduct species used (Table 2).

Table 2. Optimized IM parameters depending of the drift gas.

Gas	N_2	N_2O	CO_2	He
Wave velocity (m s^{-1})	800	400	400	600
Height velocity (V)	40	40	40	5.5
Gas flow (mL min^{-1})	90	90	90	50

Experiments were accomplished in the 'V' resolution mode (resolving power of 18,000 FWHM) in the *m/z* 50 to 600 range except for salt clusters $[GTX+Met_{n+1}+X_n]^+$ and $[GTX-H+Met_{n+2}+X_n]^+$ which were analyzed in the *m/z* range 50 to 1200.

Calibration of the Traveling Wave Ion Mobility (TWIM) cell to convert t_D to CCS values was carried out using the method detailed by Smith *et al.* [27, 28]. Polyalanine was used to calibrate the TWIM cell, and database of N_2 CCS values was used [29]. All the drift time peaks extracted from *m/z* values were fitted with a Gaussian function using the single peak fitting tool of Origin 9.1 software (OriginLab).

Theoretical calculations

Density Functional Theory (DFT) calculations were carried out with the Gaussian 09 [30] program in order to gain insight into the structures of gas phase ions. The (dispersion-corrected range-separated hybrid) ωB97X-D exchange-correlation functional [31] was used in conjunction with the 6-311++G(d,p) triple-ζ basis set for all atoms. All structures were fully optimized *in vacuo* in their singlet spin state, and the nature of the obtained stationary points was checked by (harmonic) vibrational analyses, which also generated atomic APT [32] charges. The MOBCAL software [33, 34] was used in complement to generate CCS values from these DFT optimized structures.

RESULTS AND DISCUSSION

1. *Alkali adducts formation*

Different Met^+X^- salts (Met = Li, Na, K and X = I, Cl, TFA, OH) at different concentrations (0.01, 0.1, 0.5, 1, 5 and 10 mmol L^{-1}) were examined to improve the cationization of the different GTX analogues and their influence on ion mobility separation. The most intense signals of $[GTX+Met]^+$ were obtained with either LiI at 0.5 mmol L^{-1}, NaCl at 1 mmol L^{-1} or KI at 0.5 mmol L^{-1}. Due to the epimerization of isomer pairs that naturally occurs in solution after isolation of isomers to reach an equilibrium mixture of GTX isomers with a ratio of approximately 3:1 [35], on-line separation using HILIC-IM-MS was used to characterize individual species, according to the analytical methodology previously reported for STX analogues using HILIC-IM-MS coupling [14]. In such HILIC conditions, isomers of GTXs could be separated allowing the unambiguous drift time (t_D) assignment for each GTX isomer; ion mobility spectra were individually extracted from the HILIC-IM-MS data at each specific isomer retention times. For HILIC-IM-MS experiments, three different aqueous phases were tested involving either LiI at 1 mmol L^{-1}, NaCl at 2 mmol L^{-1} or KI at 1 mmol L^{-1}. In all cases, the pH was adjusted to 3.5 with formic acid.

Mass spectra of GTX2 and GTX3 analogues were acquired following HILIC separation using a mobile phase containing 1 mmol L^{-1} or KI (Figure 1), HILIC-IM-MS experiments using LiI and NaCl are reported in Figure S1. All spectra show $[GTX+Met]^+$ adducts but also higher *m/z* salt clusters such as $[GTX+Met_{n+1}+X_n]^+$ and $[GTX-H+Met_{n+2}+X_n]^+$ (Figure 1). For example, potassium adducts $[GTX2/3+K]^+$ were detected at *m/z* 434.05 (Figure 1) and constitute the most abundant species, while higher *m/z* salt clusters were detected in lower abundance at *m/z* 472.01, *m/z* 599.92, *m/z* 765.79, *m/z* 931.66 and *m/z* 1097.52. Note that

some protonated molecules could be observed ($[GTX3+H]^+$ at *m/z* 396.09) as well as some fragment ions (*m/z* 378.08, *m/z* 316.14 and *m/z* 298.13 from $[GTX3+H]^+$ and *m/z* 316.14 from $[GTX2+H]^+$). These fragment ions involved losses of H_2O and/or SO_3 molecules from protonated species (Figure 1a, 1b and Figure S1, even using the softest voltage conditions for ion desolvation). We noticed that the neutral losses (H_2O or SO_3) varied with the nature of isomers. Thus, $[GTX4+H]^+$, $[GTX3+H]^+$ and $[dcGTX3+H]^+$ mainly fragmented loosing H_2O, while $[GTX1+H]^+$, $[GTX2+H]^+$ and $[dcGTX2+H]^+$ only exhibited loss of SO_3. $[GTX2+H]^+$ at *m/z* 396.09 could not be detected on Figure 1b, due to complete fragmentation into $[GTX2+H-SO_3]^+$, while GTX alkali adducts were abundant species and did not widely fragment, meaning that they were significantly more stable than the protonated molecules, as shown by the weak $[GTX-H_2O+Met]^+$ ion which was the sole fragment ion detected for all $[GTX+Met]^+$.

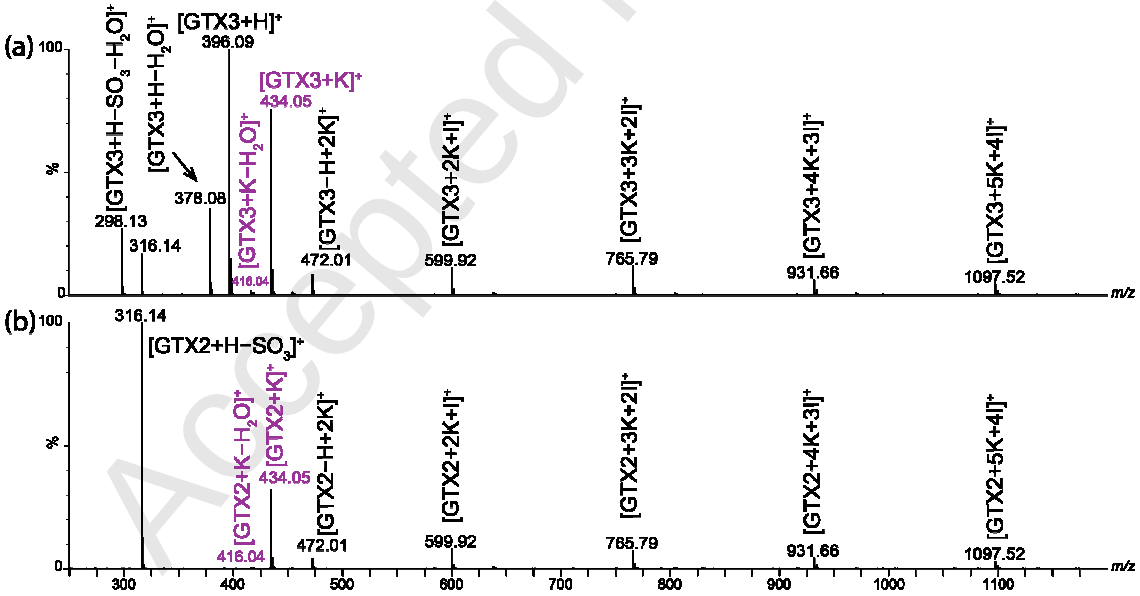

Figure 1. Mass spectra of GTX3 (a), GTX2 (b) extracted from LC-MS experiments. Solvent A: aqueous solution of KI at 1 mmol L^{-1}, adjusted to pH 3.5 with formic acid, and solvent B: acetonitrile, were used as mobile phase.

Cationic adducts of (R,S,R,S) GTXs featuring the sulfate group at the front of the molecular plane (GTX4, GTX3, dcGTX3) slightly underwent more abundant loss of H_2O than their

corresponding (R,S,R,R) isomers (GTX1, GTX2, dcGTX2). This tendency was observed independently of the nature of the alkali cation or of the GTX isomer pairs (Table S1). The neutral loss of SO_3 was not observed in the case of alkali adducts, meaning that the sulfate group was stabilized for GTX1, GTX2, and dcGTX2, probably due to an ionic interaction between the sulfate group and the Met^+ [23].

Subsequently, limits of detection (LODs) were compared for cationic and protonated molecules, estimated by HILIC-IM-MS technique (using the area of extracted ion chromatogram peaks). LODs of cationic species were found to be lower (in the range 1-2 µM) than those of protonated GTXs (in the 1-20 µM range, from standard samples). This can be explained by the fragmentation of protonated GTX1, GTX2, and dcGTX2, which do not permit the detection of intact molecular species at very low concentration. Note that the addition of the IM dimension does not indubitably induce a loss of sensitivity (less than a factor 2 in the worst case, and sometimes slight increases of sensitivity were obtained).

Thus, the formation of alkali metal ion adducts allows for the stabilization of molecular species and permits to reach lower LODs (Figure 2). Moreover, semi-quantitative analysis (n=8) could be achieved in HILIC-IM-MS; the relative proportions of each diastereomer among a pair (*i.e*. GTX2/3 or GTX1/4) could be determined. Similar values of percentages were found, regardless of the nature of the adduct (Figure 2). Moreover, quantitation can be achieved in both HILIC and IM dimension from the peak areas of the extracted ion chromatograms or the extracted ion mobility spectra.

Figure 2. Relative proportions of GTX isomers determined from HILIC-IM-MS experiments using salt addition in the mobile phase in the concentration range for GTXs of 1-20 µmol L^{-1}. Error bars correspond to twice the standard deviation value for n=8 experiments.

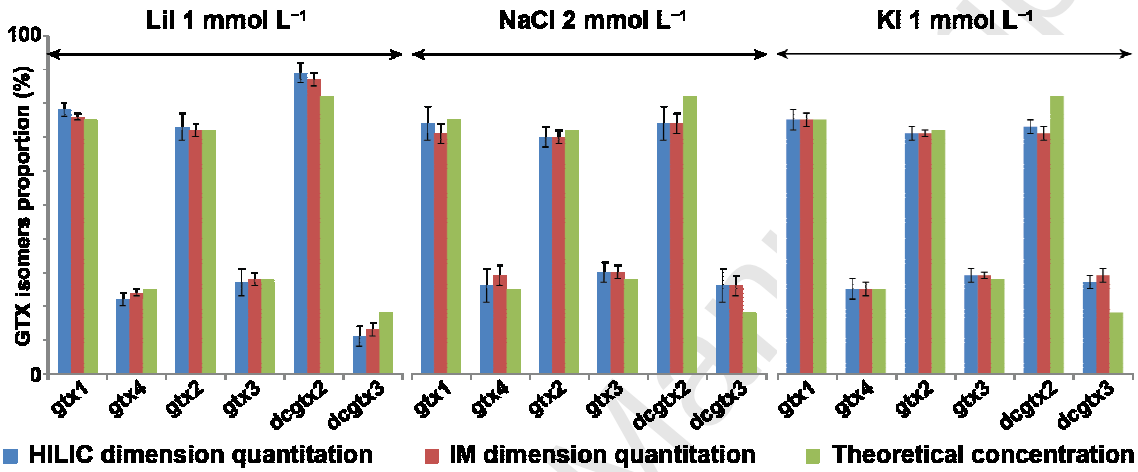

In a second phase, the elimination of the HILIC dimension was considered to reduce analysis time scale, through direct IM-MS analysis with GTX solutions infusion.

2. IM-MS separation of [GTXs+Met]$^+$

Direct infusion of salted solutions of GTXs were carried out using the same salt concentration as previously used for HILIC-IM-MS; 0.5 mmol L^{-1} toxin solutions containing either 0.5 mmol L^{-1} LiI, 1 mmol L^{-1} NaCl or 0.5 mmol L^{-1} KI were used. Even if the aim was to identify each isomer without chromatographic separation, HILIC-IM-MS separations were performed in parallel in order to ensure that the t_D of each GTX isomer was unambiguously assigned. In fact, the chromatographic separation dimension was required for the initial t_D assignment as the diastereomers do not present specific product ions that could have been used to extract specific ion mobility spectra (Figure S2).

To optimize the GTX separation in the IM dimension, three buffer gases were tested - N_2, CO_2 and N_2O - since improvements of isomer separation have been previously reported using these gases [19, 20]. IM parameters of the instrument had to be adjusted for each combination of gas and alkali adducts. Thus, depending on the gas studied, the wave height was set to either 20, 30 or 40 V, the velocity wave varied from 200 to 1600 m s^{-1} using 100 m s^{-1} step and the IM gas flow varied from 50 to 90 mL min^{-1}, using 10 mL min^{-1} step. A total of more than 15 different combinations of parameters were tested for each gas.

2.1. Comparison of alkali adducts in N_2 buffer gas

Ion mobility spectra (XIMS) of $[GTXs+Met]^+$ were acquired and extracted from IM-MS, and HILIC-IM-MS experiments were performed using N_2 as buffer gas (Figure 3). For each alkali adduct of GTXs, the XIMS were extracted either for individual diastereomer species after chromatographic separation (HILIC-IM-MS) or for the mixture with direct infusion (IM-MS). The XIMS of each isomer mixture corresponded perfectly to the superposition of the two diastereomer XIMS after HILIC separation. On the whole, excepted for $[dcGTX2/3+Li]^+$ (Figure 3a), the R,S,R,S-compounds (GTX4, GTX3 and dcGTX3, blue XIMS in Figure 3) exhibited smaller t_D than R,S,R,R-compounds (GTX1, GTX2 and dcGTX2, green XIMS in Figure 3). Therefore, R,S,R,S-compounds showed more folded conformations in the gas phase than R,S,R,R-analogues.

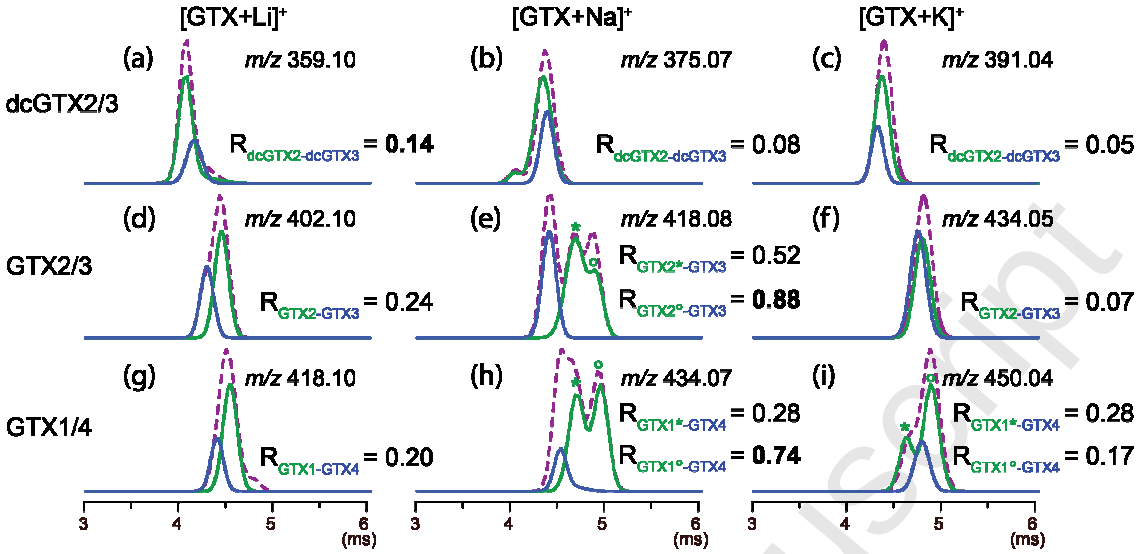

Figure 3. Ion mobility spectra observed in N_2 in the following conditions: wave velocity 800 m s^{-1}, height wave 40 V and gas flow 90 mL min^{-1}. Green XIMS correspond to dcGTX2, GTX1 or GTX2 (R,S,R,R), extracted from HILIC-IM-MS experiments and blue XIMS to dcGTX3, GTX4 or GTX3 (R,S,R,S). Purple dashed XIMS correspond to the mixtures of diastereomers of dcGTX2/3, GTX1/4 or GTX2/3, extracted from direct infusion experiments.

Different behavior was obtained depending on the alkali metal (Figure 3). No diastereomer separation could be evidenced from the isomer mixtures of $[GTXs+Li]^+$ (purple dashed XIMS Figure 3a, 3d and 3g) due to a lack of IM resolution.

GTX sodium adducts present more complex ion mobility spectra (Figure 3). Only one signal was obtained from (R,S,R,S) $[GTXs+Na]^+$ (blue XIMS Figure 3b, 3e and 3h) compounds as was observed for (R,S,R,S) $[GTXs+Li]^+$ and $[GTXs+K]^+$. However, XIMS from (R,S,R,R) isomers of $[GTXs+Na]^+$ (green XIMS Figure 3b, 3e and 3h) showed two or three partially resolved signals. The corresponding different t_D can be related to different cationization sites on the molecule, but also to repulsion that can occur between the cation and the carbamoyl moiety. This hypothesis is supported by the presence of only two IM peaks for $[dcGTX2+Na]^+$ (Figure 3b) which do not possess a carbamoyl function. In that case, the peak of lower mobility of $[GTX2+Na]^+$ (t_D = 4.97 ms) and of $[GTX1+Na]^+$ (t_D = 5.04 ms) (green XIMS Figure 3e and 3h) could correspond to possible conformations for chelated metal.

Concerning the $[GTXs+K]^+$ species, no separation was obtained for dcGTX2/3 and GTX2/3 while the diastereomers of the GTX1/4 pair showed two different IM spectra. In fact, $[GTX1+K]^+$ exhibited two IM peaks while $[GTX4+K]^+$ only presented a peak positioned between the two $[GTX1+K]^+$ peaks (Figure 3i).

Furthermore, some peak tails were observed for *m/z* 359.10, 402.10 and 418.10 in the direct infusion experiments that were not observed in the XIMS obtained after chromatographic separation. These peak tails were due to the presence of unseparated contaminants which were isobaric species, as mentioned in the experimental section and depicted in the supporting information, Figure S3.

2.2. Comparison of N_2, N_2O and CO_2 buffer gases

In this part, several drift gases presenting different polarizabilities were compared in order to improve the ion mobility separation. As a selection of all data, XIMS from IM-MS and HILIC-IM-MS experiments were obtained for $[dcGTX2/3+Na]^+$, $[GTX2/3+Li]^+$ and $[GTX1/4+K]^+$ in N_2, N_2O and CO_2 drift gases (Figure 4). The results corresponding to the other adducts are presented in Figure S4 and S5 in the supplementary information.

Overall, changing the buffer gas did not significantly improve the separation of diastereomers. For instance, $[dcGTX2/3+Na]^+$ did not show an improvement in isomer separation but only larger IM peaks (Figure 4a). The species $[GTX2/3+Li]^+$ and $[GTX1/4+K]^+$ presented the best differences for different gases (Figure 4b and 4c). For these two isomeric pairs, the use of N_2O and CO_2 as drift gas improved the separation of both isomer pairs without changing the t_D order.

From the IM optimizations, changing either alkali ion or buffer gases, it appears to be more efficient and easier to change the alkali metal nature than the drift gas. Firstly, changing the alkali metal only took minutes and was effective for all diastereomer pairs. Sodiated adducts

showed more isomer differentiation in N_2 gas than lithium and potassium adducts with all drift gases studied (Figure 3). Furthermore, changing buffer gas is more complex to implement, from a technical point of view, and does not yield predictable results. Hence, improvements of the separation were not systematically observed, but rather sporadically.

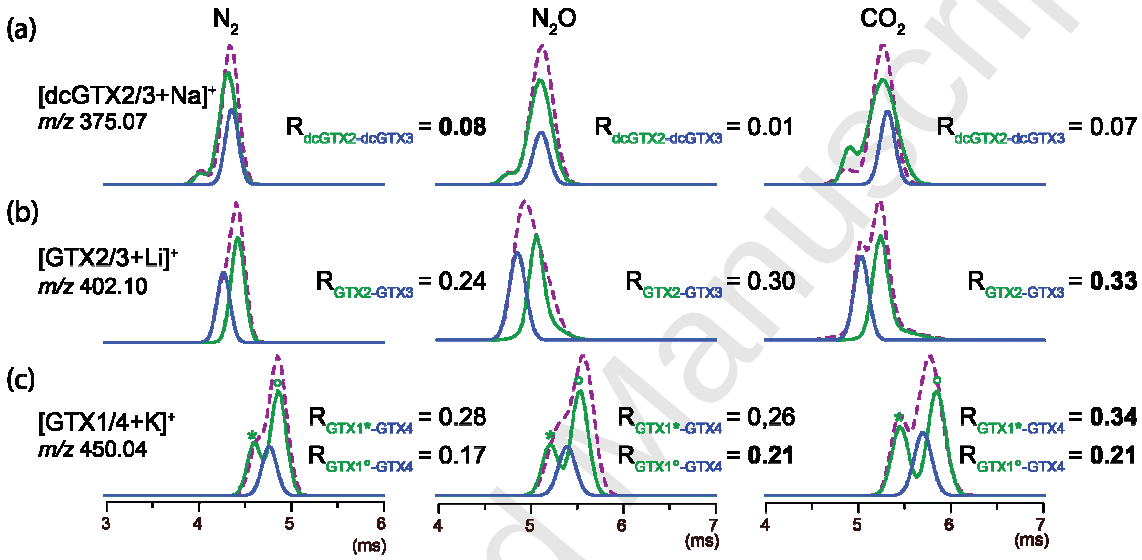

Figure 4. XIMS of $[dcGTX2/3+Na]^+$ *m/z* 375.07, $[GTX2/3+Li]^+$ *m/z* 402.10 and $[GTX1/4+K]^+$ *m/z* 450.04 in N_2, N_2O and CO_2 drift gases from IM-MS and HILIC-IM-MS. In purple dashed, XIMS obtained from mixtures in direct introduction. In green, dcGTX2, GTX2 and GTX1 (R,S,R,R); in blue, dcGTX3, GTX3 and GTX4 (R,S,R,S) XIMS extracted from HILIC-IM-MS experiments.

In addition to the IM separation optimization in the positive ionization mode, $[GTX-H]^-$ species were also studied because of their higher stability compared to $[GTX+H]^+$ [23]. $[GTX-H]^-$ in N_2, N_2O and CO_2 were studied in (HILIC)-IM-MS but the improvement of the separation observed was not sufficient to allow for complete separation (Figure S6, Figure S7 and Table S2).

3. IM-MS separation of $[GTXs+Met-H_2O]^+$

From IM-MS/MS analysis of $[GTXs+Met]^+$, XIMS of the most intense product ions $[GTXs+Met-H_2O]^+$ and $[GTXs+Met-SO_3]^+$ were extracted. As the loss of sulfate group occurred on the stereocenter, the resulting IM experiments did not improve the separation. In contrast, XIMS of $[GTXs-H_2O+Met]^+$ from IM-MS experiments, showed profiles different to those of $[GTXs+Met]^+$ species (Figure 3 compared to Figure 5). The loss of water likely occurred on the doubly-hydroxylated carbon as the loss of water on the carbamoyl moiety seems energetically unfavourable [36].

To obtain ion mobility separation of fragment ions, precursor ion activation has to occur in the trap cell located before the ion mobility cell [37]. (HILIC-)IM-MS/MS spectra were obtained testing different collision energies (from 10 to 20 eV, with Ar as the collision gas). Abundant loss of H_2O was observed from as little as 10 eV collision energy in the case of $[GTXs+Li]^+$ and $[GTXs+Na]^+$ species while 20 eV collision energy was necessary to generate $[GTXs+K-H_2O]^+$ product ions of each isomer pairs. For all the alkali salts and GTXs studied, two main IM peaks were observed for infused diastereoisomer mixtures (purple dashed XIMS in Figure 5). The peak showing the smallest t_D (near 4ms) of every isomer pair in mixture is always more intense while the peak of higher t_D (near 5ms) is less intense and broader. When isomers are separated (HILIC-IM-MS/MS experiments performed in parallel to infusion IM-MS/MS), the R,S,R,S-compounds (GTX4, GTX3 and dcGTX3, blue XIMS in Figure 5) correspond to the IM peak of higher mobility (smallest t_D, near 4ms). On the other hand, the R,S,R,R-compounds (GTX1, GTX2 and dcGTX2, green XIMS in Figure 5) show two or even three IM peaks, the most intense corresponding to the peak of higher t_D, previously observed in the mixture (the peak(s) of smaller t_D is(are) always minor). Three peaks are only observed for sodiated adducts of GTX2 and dcGTX2 (Figure 5b and 5e). These results can be explained with regard to the XIMS of the sodium adducts which were complex; two partially resolved signals were observed (Figure 3e and 3h). Moreover, the

detection of two IM peaks for $[GTXs+Met-H_2O]^+$ ions can also be explained by epimerization that can occur in the fragmentation pathway involving the loss of H_2O. Note that the t_D observed for the $[GTXs+Met-H_2O]^+$ can be more important than those of the precursor $[GTXs+Met]^+$ ions.

However, the differentiation of isomers is possible in certain cases, by extracting XIMS of some $[GTXs+Met-H_2O]^+$ product ions and examining both t_D and peak intensity, with Met = potassium or lithium (Figure 5). Therefore, $[GTXs+K-H_2O]^+$ appears helpful to differentiate GTX1 from GTX4 and dcGTX2 from dcGTX3, while $[GTXs+Li-H_2O]^+$ permits to differentiate GTX1 from GTX4 and GTX2 from GTX3. Thus IM-MS/MS analyses of GTXs allow for the identification of each GTX, including diastereomer detection.

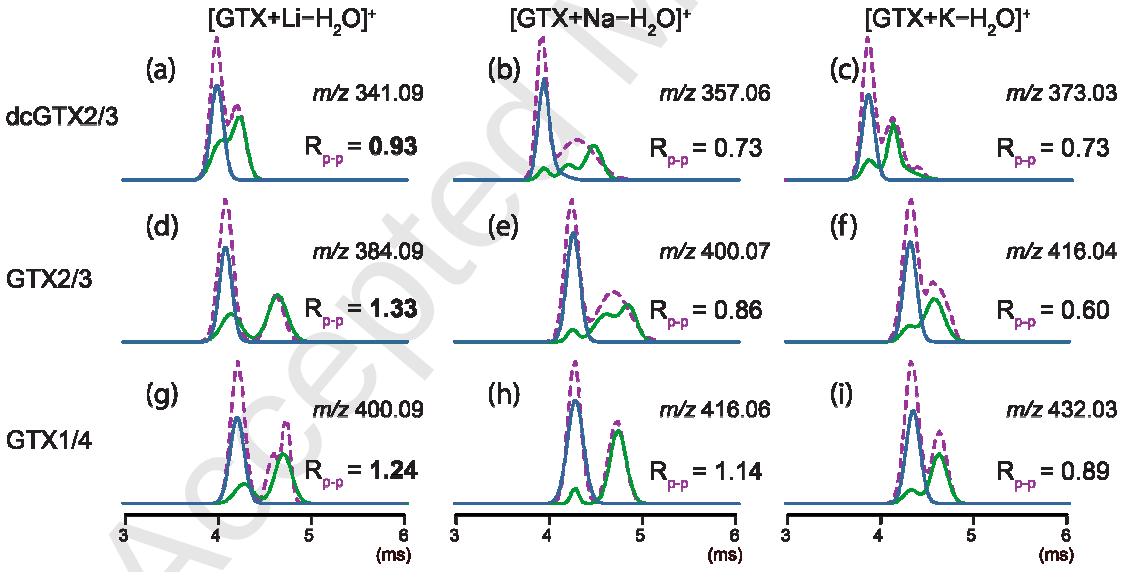

Figure 5. XIMS observed in N_2 using 10 eV collision energy in the trap cell for $[GTXs+Li-H_2O]^+$ and $[GTXs+Na-H_2O]^+$ product ions, 20 eV for $[GTXs+K-H_2O]^+$. Green XIMS correspond to dcGTX2, GTX1 or GTX2 (R,S,R,R), and blue XIMS to dcGTX3, GTX4 or GTX3 (R,S,R,S) from HILIC-IM-MS/MS experiments. Purple dashed XIMS correspond to the mixtures of diastereomers of dcGTX2/3, GTX1/4 or GTX2/3, extracted from IM-MS/MS experiments. R_{p-p} are calculated from direct introduction experiments, bold values correspond to highest resolution of separation.

We can note that the peak to peak resolution R_{p-p} values increase when the size of the cation decreases for each studied isomer pair ($R_{p-p}Li > R_{p-p}Na > R_{p-p}K$). The $[GTXs+Li-H_2O]^+$

species show then the best resolution with values comprised between 0.93 and 1.33 (Figure 5a, 5d and 5g).

As previously mentioned, the ion mobilities of $[GTX+Met]^+$ and $[GTX-H_2O+Met]^+$ were close. Therefore, to ensure that the IM peaks observed in Figure 5 specifically correspond to $[GTX-H_2O+Met]^+$ and do not result from dissociation of metastable $[GTX+Met]^+$ ions that could fragment after IM separation, in-source CID experiments with isolation of the $[GTX-H_2O+Met]^+$ ions in the quadrupole were performed and compared to CID experiments in the trap cell after $[GTX+Met]^+$ isolation.

Ion mobility profiles were obtained for $[GTX2+Li]^+$, $[GTX3+Li]^+$, $[GTX2-H_2O+Li]^+$ and $[GTX3-H_2O+Li]^+$ in HILIC-IM-MS/MS conditions, with product ions being generated in the trap cell or in the source of the instrument (Figure 6). Figure 6b shows the $[GTX-H_2O+Met]^+$ generated in the trap cell from selected $[GTX+Met]^+$, separated by IM, and mass analyzed. In addition, Figure 6c shows $[GTX-H_2O+Met]^+$ generated in the ESI source, isolated by the quadrupole, separated by IM, and mass analyzed.

The XIMS of $[GTX3-H_2O+Li]^+$ ion show a peak at 4.1 ms slightly lower than the peak of the precursor $[GTX3+Li]^+$ ion, in both cases (in-source CID and CID in the trap cell) confirming that the previously observed IM peak in Figure 5 corresponded to $[GTX3-H_2O+Li]^+$ ion. The same conclusion could be given for GTX2, even if two peaks are still observed at different intensities; indeed, the resulting $[GTX2-H_2O+Li]^+$ ions showed two peaks at 4.1 and 4.6 ms, in both CID conditions but with different intensities (Figure 6b and 6c). XIMS obtained with trap cell activation present a more intense peak at (t_D = 4.6 ms) while XIMS obtained with in-source activation shows a more intense peak (t_D = 4.1 ms). These differences in intensities can be explained by *(i)* different time windows, *(ii)* different activation conditions due to collision with different gases in the trap cell (Ar) and in source (N_2) or *(iii)* gas phase rearrangement of the ion.

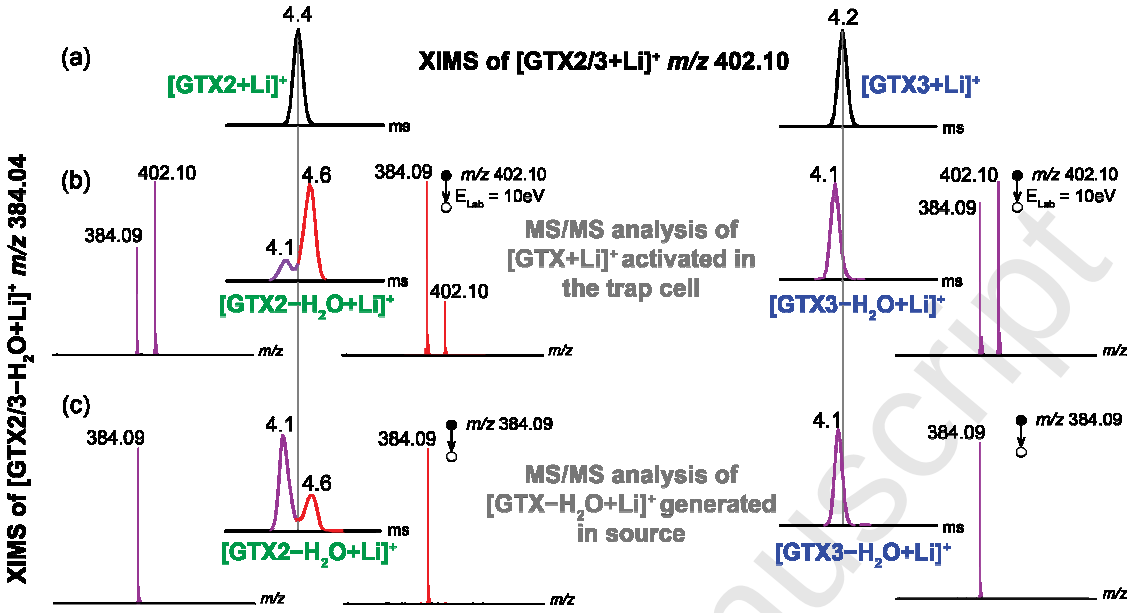

Figure 6. (a) XIMS of $[GTX2/3+Li]^+$, (b) IM separation of $[GTX2/3-H_2O+Li]^+$ generated from $[GTX2/3+Li]^+$ after activation in the trap cell of the instrument, and (c) IM separation of $[GTX2/3-H_2O+Li]^+$ generated in source and selected in the quadrupole.

This methodology allows for a fast identification of all isomers but the LC dimension is still necessary to quantify isomer mixtures if no calibration curve is done, as the different t_D are not specific.

4. Theoretical calculations

In order to correlate experimental data to theoretical structures, experimental CCS values of $[GTXs+Met]^+$ species were determined (Table 3). It can be seen from these values that for $[dcGTX2/3+Met]^+$, sodium and potassium adducts are very similar, while lithiated species are much smaller. This tendency is also observed for $[GTX3+Met]^+$ and $[GTX4+Met]^+$. In contrast, $[GTX1+Met]^+$ and $[GTX2+Met]^+$ shows an increase of CCS values in linearly function of the cation size (Li < Na < K). These results suggest a common cationization site for $[GTX1+Met]^+$ and $[GTX2+Met]^+$.

Table 3. Experimental CCS obtained using N_2 as buffer gas and polyalanine calibration using N_2 polyalanine values.

	CCSexp of $[GTXs+Met]^+$ ($Å^2$)		
	Li	Na	K
$[dcGTX2+Met]^+$	181	180/188	188
$[dcGTX3+Met]^+$	183	188	187
$[GTX2+Met]^+$	189	189/195/200	198
$[GTX3+Met]^+$	185	188	197
$[GTX1+Met]^+$	191	190/195/201	193/199
$[GTX4+Met]^+$	188	191	197

DFT calculations were carried out for all $[GTX2/3+Met]^+$ analogues (with the three alkali cations), and different coordination sites were observed depending on the isomer (selected representative structures for $[GTX2+Na]^+$ are depicted in Figure S10), almost exclusively in a polydentate coordination mode. Both $[GTX2+Met]^+$ and $[GTX3+Met]^+$ showed favored interaction between the metal and oxygen of the sulfate group. In addition, most of the lowest energy $[GTX2+Met]^+$ generated structures involved interaction with the amine group of the six-membered ring, while the $[GTX3+Met]^+$, which displayed stable conformations that are much closer in energy than in the GTX2 case, showed preferential interactions with the carbamoyl and hydroxyl moieties (Figure 7). For $[GTX3+Na]^+$, folding of the structure was observed due to the carbamoyl chelation while for $[GTX2+Na]^+$, the carbamoyl moiety is unfolded. The folding conformation generally corresponds to the smallest CCS values, which corresponds to experimental values CCS $[GTX3+Na]^+$ < CCS $[GTX2+Na]^+$ (Table 3).

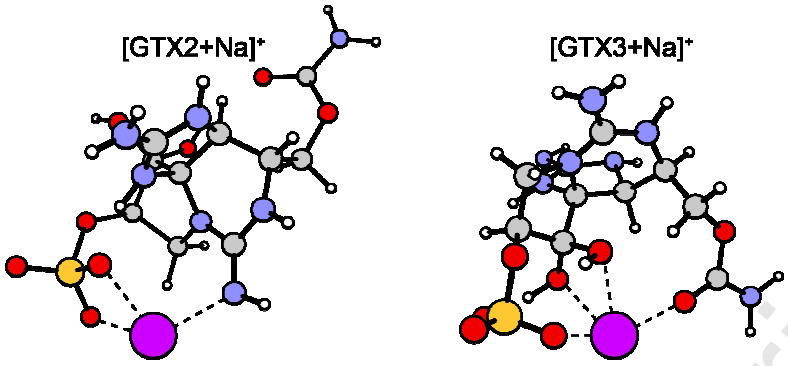

Figure 7. Representation of the sodium chelation for the lowest energy (in terms of E_{ZPE}) optimized structures of $[GTX2+Na]^+$ (E_{ZPE} = -1936.3832 E_h) on the left and $[GTX3+Na]^+$ (E_{ZPE} = -1936.3667 E_h) on the right. Carbon atoms in grey, hydrogen atoms in white, nitrogen atoms in blue, oxygen atoms in red sulfur in yellow, and sodium atom is colored in purple.

Subsequently, theoretical CCS values of optimized structures where generated using the MOBCAL software. A systematic inversion of the theoretical CCS values compared to the experimental CCS was observed. Many calibrations of the protocol (including the full DFT calculations on numerous structures stemming from the extensive sampling on the potential energy surface by a simulated annealing procedure based on the PM6 quantum semi-empirical method), the fine tuning of MOBCAL parameters [19] and code [38] (Table S3), the use of He as buffer gas (Figure S8), the variation of voltages to generate the most stable structure (Figure S9)[39]) were carried out to circumvent this inversion without success.

The lack of correlation may be due to the high polarity and polarizability of the $[GTXs+Met]^+$ structures in addition with the small CCS differences inside the isomer pairs. In fact, IM separation is based on the interactions with a buffer gas which is a polarizable gas in this study. In the case of $[GTXs+Met]^+$, separation was not observed when helium was used as buffer gas while more polarizable gases (N_2, CO_2 and N_2O) allowed for separation. The differentiation observed in IM using gases like N_2 can be explained by the molecular dipole moment that is higher for $[GTX3+Met]^+$ than $[GTX2+Met]^+$ (Table 4) resulting in different IM separation. The polarity of the ions will increase ion-dipole interactions and as a consequence, differentiate isomers in function of the polarity in addition to shape separation.

Table 4. Mean molecular polarizabilities (calculated as third the trace of the static polarizability tensor) and molecular dipole moments of $[GTX2+Met]^+$ and $[GTX3+Met]^+$ averaged for the three lowest energies (in terms of E_{ZPE}) structures generated by the quantum chemical protocol.

	$[GTX+Li]^+$		$[GTX+Na]^+$		$[GTX+K]^+$	
Toxin	Pol. ($Å^3$)	$\|\vec{d}\|$ (Debye)	Pol. ($Å^3$)	$\|\vec{d}\|$ (Debye)	Pol. ($Å^3$)	$\|\vec{d}\|$ (Debye)
GTX2	29.93	13.1	30.17	13.4	30.95	13.6
GTX3	30.10	17.4	30.23	17.7	31.07	17.4

CONCLUSION

In this work, we showed that alkali adducts of GTXs are more stable than protonated molecules allowing for lower LODs as well as the determination of relative proportions of each diastereomer in a mixture. Using IM-MS, fast separation of different analogues of gonyautoxins can be achieved using alkali metal ion adducts, $[GTXs+Met]^+$.

However, separation of $[dcGTX2/3+Met]^+$ in mixtures could not be achieved using IM-MS even after changing the nature of the IM buffer gas. On the other hand, the study of $[GTXs+Met-H_2O]^+$ showed that a discrimination of diastereomers could be obtained from IM-MS experiments in N_2 buffer gas. The highest resolution regarding the IM peaks was obtained for $[GTXs+Li-H_2O]^+$ ions with resolution of 0.9 and 1.3.

IM-MS analyses without upstream HILIC separation allowed for a discrimination of alkali adducts of GTX2/3 and GTX1/4 isomer pairs while a differentiation of dcGTX2/3 was observed only for the fragment ion arising from the loss of a H_2O molecule. The tiny CCS differences between the isomers did not lead to a satisfactory correlation between experimental and theoretical structures generated by DFT. The limitation of the model may be explained, at least in part, by the high polarity and polarizability of the ions, yielding a more complex separation mechanism.

ACKNOWLEDGEMENTS

The authors gratefully thank the Région Haute Normandie, the Direction Générale de l'Armement (DGA), the European regional development fund (ERDF) N°31708, the Labex SynOrg (ANR-11-LABX-0029) for financial support, and the "Centre de ressources informatiques de Haute-Normandie" (CRIHAN) center for computational resources.

REFERENCES

[1] S. Cestele, W.A. Catterall, Molecular mechanisms of neurotoxin action on voltage-gated sodium channels, Biochimie, 82 (2000) 883-892.
[2] J. Wang, J.J. Salata, P.B. Bennett, Saxitoxin Is a Gating Modifier of hERG K+ Channels, The Journal of General Physiology, 121 (2003) 583-598.
[3] A.P. Thottumkara, W.H. Parsons, J. Du Bois, Saxitoxin, Angew Chem Int Ed Engl, 53 (2014) 5760-5784.
[4] M. Santos, P.R. Costa, F.M. Porteiro, M.T. Moita, First report of a massive bloom of Alexandrium minutum (Dinophyceae) in middle North Atlantic: a coastal lagoon in S. Jorge Island, Azores, Toxicon, 90 (2014) 265-268.
[5] A. Negri, L. Llewellyn, J. Doyle, N. Webster, D. Frampton, S. Blackburn, Paralytic Shellfish Toxins Are Restricted to Few Species among Australia's Taxonomic Diversity of Cultured Microalgae1, J. Phycol., 39 (2003) 663-667.
[6] M. Wiese, P.M. D'Agostino, T.K. Mihali, M.C. Moffitt, B.A. Neilan, Neurotoxic Alkaloids: Saxitoxin and Its Analogs, Mar. Drugs, 8 (2010) 2185-2211.
[7] A.A. Genenah, Y. Shimizu, Specific toxicity of paralytic shellfish poisons, J. Agric. Food Chem., 29 (1981) 1289-1291.
[8] P.R. Costa, T. Moita, S.M. Rodrigues, Estimating the contribution of N-sulfocarbamoyl paralytic shellfish toxin analogs GTX6 and C3+4 to the toxicity of mussels (Mytilus galloprovincialis) over a bloom of Gymnodinium catenatum, Harmful Algae, 31 (2014) 35-40.
[9] J.F. Lawrence, B. Niedzwiadek, Quantitative determination of paralytic shellfish poisoning toxins in shellfish by using prechromatographic oxidation and liquid chromatography with fluorescence detection, J. AOAC Int., 84 (2001) 1099-1108.
[10] Y. Oshima, Postcolumn derivatization liquid chromatography method for paralytic shellfish toxins, J.AOAC Int., 78 (1995) 528-532.
[11] C. Dell'Aversano, P. Hess, M.A. Quilliam, Hydrophilic interaction liquid chromatography–mass spectrometry for the analysis of paralytic shellfish poisoning (PSP) toxins, J. Chromatogr. A, 1081 (2005) 190-201.
[12] M.A. Quilliam, M. Janeček, J.F. Lawrence, Characterization of the oxidation products of paralytic shellfish poisoning toxins by liquid chromatography/mass spectrometry, Rapid Commun. Mass Spectrom., 7 (1993) 482-487.
[13] Y. Wu, A.Y. Ho, P.Y. Qian, K.S. Leung, Z. Cai, J.M. Lin, Determination of paralytic shellfish toxins in dinoflagellate Alexandrium tamarense by using isotachophoresis/capillary electrophoresis, J. Sep. Sci., 29 (2006) 399-404.
[14] S. Poyer, C. Loutelier-Bourhis, G. Coadou, F. Mondeguer, J. Enche, A. Bossee, P. Hess, C. Afonso, Identification and separation of saxitoxins using hydrophilic interaction liquid chromatography coupled to traveling wave ion mobility-mass spectrometry, J. Mass Spectrom., 50 (2015) 175-181.

[15] D.G. Beach, J.E. Melanson, R.W. Purves, Analysis of paralytic shellfish toxins using high-field asymmetric waveform ion mobility spectrometry with liquid chromatography-mass spectrometry, Anal. Bioanal. Chem., 407 (2015) 2473-2484.
[16] V. Domalain, V. Tognetti, M. Hubert-Roux, C. Lange, L. Joubert, J. Baudoux, J. Rouden, C. Afonso, Role of Cationization and Multimers Formation for Diastereomers Differentiation by Ion Mobility-Mass Spectrometry, J. Am. Soc. Mass Spectrom., 24 (2013) 1437-1445.
[17] H. Li, K. Giles, B. Bendiak, K. Kaplan, W.F. Siems, H.H. Hill, Jr., Resolving structural isomers of monosaccharide methyl glycosides using drift tube and traveling wave ion mobility mass spectrometry, Anal. Chem., 84 (2012) 3231-3239.
[18] V. Domalain, M. Hubert-Roux, C.M. Lange, J. Baudoux, J. Rouden, C. Afonso, Use of transition metals to improve the diastereomers differentiation by ion mobility and mass spectrometry, J. Mass Spectrom., 49 (2014) 423-427.
[19] P.M. Lalli, Y.E. Corilo, M. Fasciotti, M.F. Riccio, G.F. de Sa, R.J. Daroda, G.H. Souza, M. McCullagh, M.D. Bartberger, M.N. Eberlin, I.D. Campuzano, Baseline resolution of isomers by traveling wave ion mobility mass spectrometry: investigating the effects of polarizable drift gases and ionic charge distribution, J. Mass Spectrom., 48 (2013) 989-997.
[20] A.B. Kanu, H.H. Hill, Jr., Identity confirmation of drugs and explosives in ion mobility spectrometry using a secondary drift gas, Talanta, 73 (2007) 692-699.
[21] T.D. Fridgen, Infrared consequence spectroscopy of gaseous protonated and metal ion cationized complexes, Mass Spectrom. Rev., 28 (2009) 586-607.
[22] T.G. Flick, I.D. Campuzano, M.D. Bartberger, Structural resolution of 4-substituted proline diastereomers with ion mobility spectrometry via alkali metal ion cationization, Anal. Chem., 87 (2015) 3300-3307.
[23] F.A. Dorr, B. Kovacevic, Z.B. Maksic, E. Pinto, D.A. Volmer, Intriguing differences in the gas-phase dissociation behavior of protonated and deprotonated gonyautoxin epimers, J. Am. Soc. Mass Spectrom., 22 (2011) 2011-2020.
[24] K. Giles, J.P. Williams, I. Campuzano, Enhancements in travelling wave ion mobility resolution, Rapid Commun. Mass Spectrom., 25 (2011) 1559-1566.
[25] A.A. Shvartsburg, R.D. Smith, Fundamentals of traveling wave ion mobility spectrometry, Anal. Chem., 80 (2008) 9689-9699.
[26] Y. Zhong, S.J. Hyung, B.T. Ruotolo, Characterizing the resolution and accuracy of a second-generation traveling-wave ion mobility separator for biomolecular ions, Analyst, 136 (2011) 3534-3541.
[27] D.P. Smith, T.W. Knapman, I. Campuzano, R.W. Malham, J.T. Berryman, S.E. Radford, A.E. Ashcroft, Deciphering drift time measurements from travelling wave ion mobility spectrometry-mass spectrometry studies, Eur. J. Mass Spectrom., 15 (2009) 113-130.
[28] C.B. Lietz, Q. Yu, L. Li, Large-scale collision cross-section profiling on a traveling wave ion mobility mass spectrometer, J. Am. Soc. Mass Spectrom., 25 (2014) 2009-2019.
[29] M.F. Bush, I.D. Campuzano, C.V. Robinson, Ion mobility mass spectrometry of peptide ions: effects of drift gas and calibration strategies, Anal. Chem., 84 (2012) 7124-7130.
[30] M.J. Frisch, G.W. Trucks, H.B. Schlegel, G.E. Scuseria, M.A. Robb, J.R. Cheeseman, G. Scalmani, V. Barone, B. Mennucci, G.A. Petersson, H. Nakatsuji, M. Caricato, X. Li, H.P. Hratchian, A.F. Izmaylov, J. Bloino, G. Zheng, J.L. Sonnenberg, M. Hada, M. Ehara, K. Toyota, R. Fukuda, J. Hasegawa, M. Ishida, T. Nakajima, Y. Honda, O. Kitao, H. Nakai, T. Vreven, J.A. Montgomery Jr., J.E. Peralta, F. Ogliaro, M.J. Bearpark, J. Heyd, E.N. Brothers, K.N. Kudin, V.N. Staroverov, R. Kobayashi, J. Normand, K. Raghavachari, A.P. Rendell, J.C. Burant, S.S. Iyengar, J. Tomasi, M. Cossi, N. Rega, N.J. Millam, M. Klene, J.E. Knox, J.B. Cross, V. Bakken, C. Adamo, J. Jaramillo, R. Gomperts, R.E. Stratmann, O. Yazyev, A.J. Austin, R. Cammi, C. Pomelli, J.W. Ochterski, R.L. Martin, K. Morokuma, V.G. Zakrzewski, G.A. Voth, P. Salvador, J.J. Dannenberg, S. Dapprich, A.D. Daniels, Ö. Farkas, J.B.

Foresman, J.V. Ortiz, J. Cioslowski, D.J. Fox, Gaussian 09, in, Gaussian, Inc., Wallingford, CT, USA, 2009.
[31] J.D. Chai, M. Head-Gordon, Long-range corrected hybrid density functionals with damped atom-atom dispersion corrections, Phys. Chem. Chem. Phys., 10 (2008) 6615-6620.
[32] J. Cioslowski, A new population analysis based on atomic polar tensors, J. Am. Chem. Soc., 111 (1989) 8333-8336.
[33] A.A. Shvartsburg, M.F. Jarrold, An exact hard-spheres scattering model for the mobilities of polyatomic ions, Chem. Phys. Lett., 261 (1996) 86-91.
[34] M.F. Mesleh, J.M. Hunter, A.A. Shvartsburg, G.C. Schatz, M.F. Jarrold, Structural Information from Ion Mobility Measurements: Effects of the Long-Range Potential, J. Phys. Chem., 100 (1996) 16082-16086.
[35] L.M. Botana, Seafood and freshwater toxins, (2000).
[36] Y. Kasetti, P. Bharatam, Tautomerism in drugs with benzimidazole carbamate moiety: an electronic structure analysis, Theor. Chem. Acc., 131 (2012) 1-12.
[37] H. Li, B. Bendiak, W.F. Siems, D.R. Gang, H.H. Hill, Determining the Isomeric Heterogeneity of Neutral Oligosaccharide-Alditols of Bovine Submaxillary Mucin Using Negative Ion Traveling Wave Ion Mobility Mass Spectrometry, Anal. Chem., 87 (2015) 2228-2235.
[38] I. Campuzano, M.F. Bush, C.V. Robinson, C. Beaumont, K. Richardson, H. Kim, H.I. Kim, Structural characterization of drug-like compounds by ion mobility mass spectrometry: comparison of theoretical and experimentally derived nitrogen collision cross sections, Anal. Chem., 84 (2012) 1026-1033.
[39] Z. Hall, A. Politis, M.F. Bush, L.J. Smith, C.V. Robinson, Charge-State Dependent Compaction and Dissociation of Protein Complexes: Insights from Ion Mobility and Molecular Dynamics, J. Am. Chem. Soc., 134 (2012) 3429-3438.
[40] http://www.indiana.edu/~nano/software.html, in.

Supplementary material

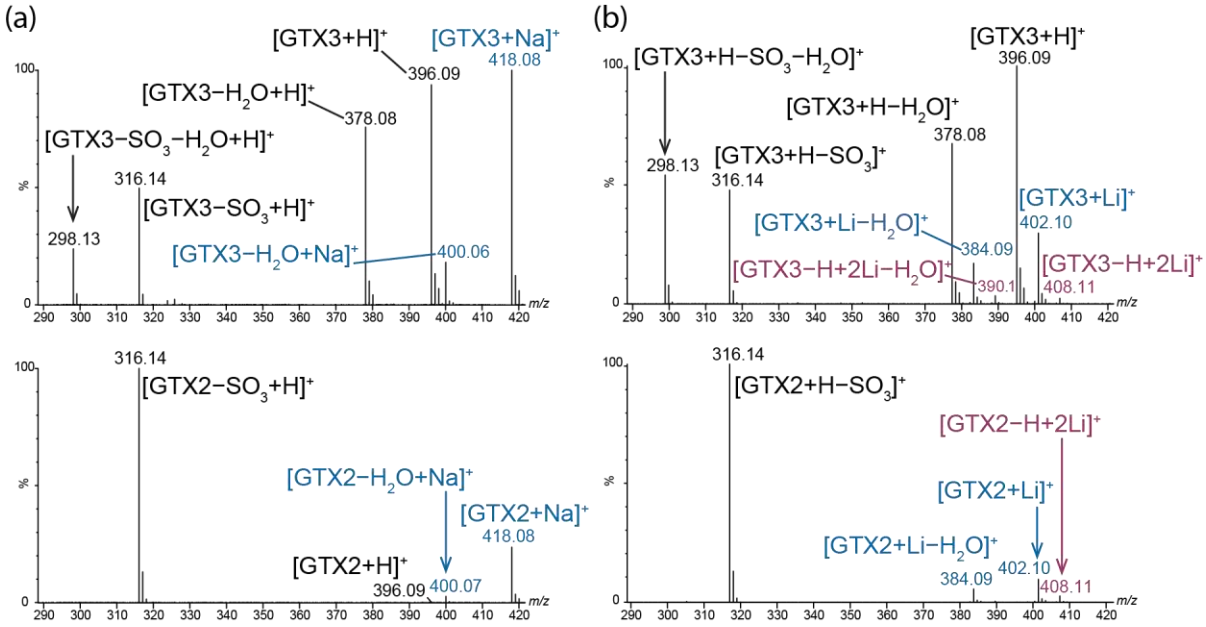

Figure S1
MS spectra of GTX2 and GTX3 extracted from HILIC-MS experiment with a background subtraction. A solution of (a) NaCl at 2 mmol L^{-1} pH 3.5, (b) LiI at 1 mmol L^{-1} pH 3.5, and acetonitrile were used as mobile phase.

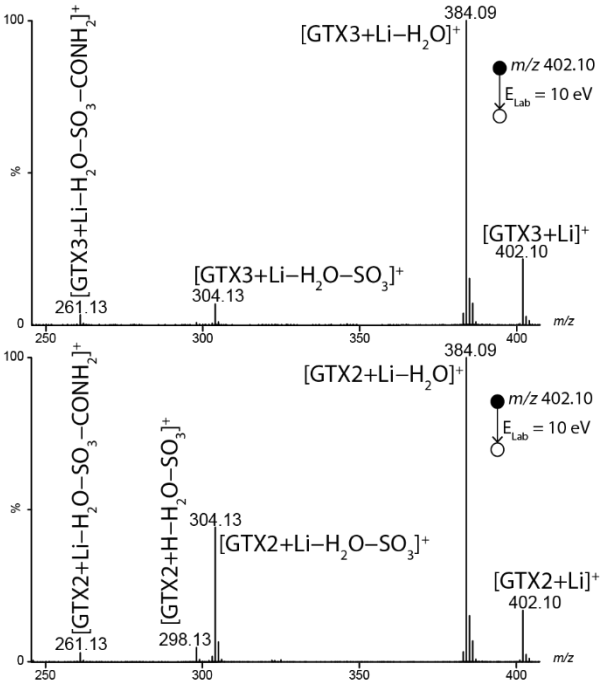

Figure S2. MS/MS spectra using 10 V of activation energy in the trap cell of lithiated GTX2 and GTX3 extracted from HILIC-MS experiment with a background subtraction. A solution of LiI at 1 mmol L^{-1} adjusted at pH 3.5 with formic acid was used as aqueous mobile phase.

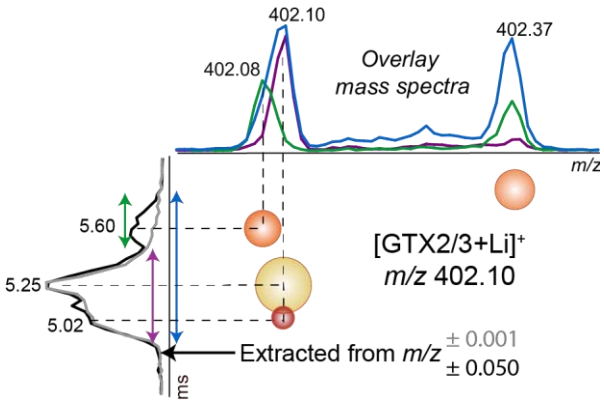

Figure S3. XIMS of *m/z* 402.10 in function of corresponding mass spectra extracted from different t_D using CO_2 as drift gas. The sphere size and color are dependent of the ion intensity value extracted from peak detection tool; yellow corresponds to the most intense signal, red corresponds to the less intense signal.
XIMS were obtained from extracted *m/z* values and in the example of $[GTX2/3+Li]^+$, the time-of-flight analyzer in 'V resolution' mode is not sufficient to allow the separation of the two isobaric species at *m/z* 402.10 and *m/z* 402.08.

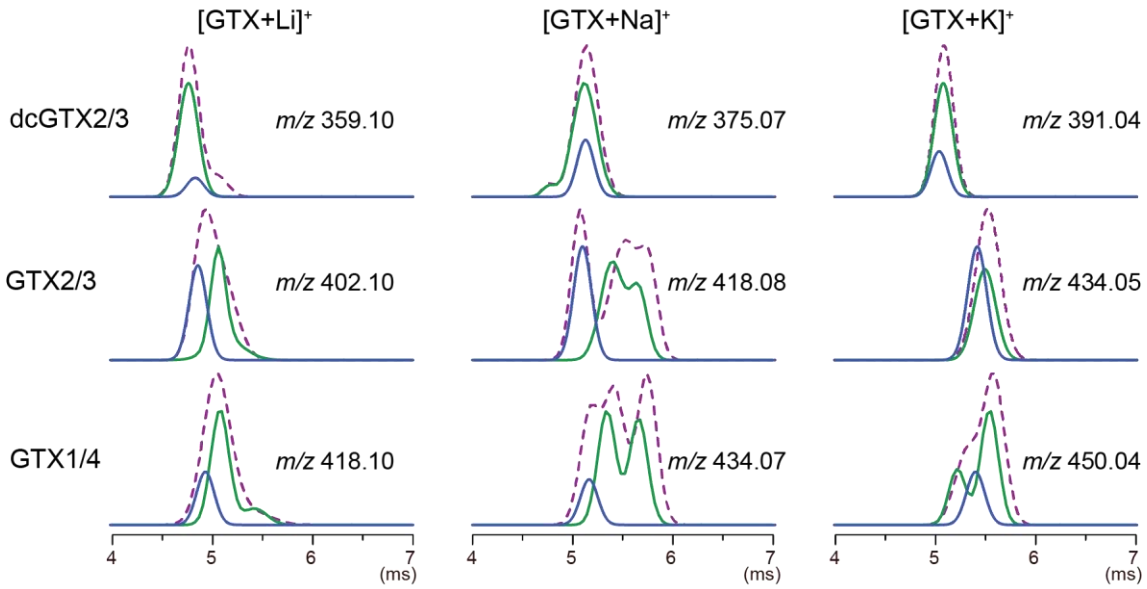

Figure S4. IM spectra observed in N_2O in the following conditions: wave velocity 400 m s^{-1}, height wave 40 V and gas flow 90 mL min^{-1}. Green XIMS correspond to dcGTX2, GTX1 or GTX2, extracted from HILIC-IM-MS experiments and blue XIMS to dcGTX3, GTX4 or GTX3. Dashed purple XIMS correspond to the mixtures of diastereomers of dcGTX2/3, GTX1/4 or GTX2/3, extracted from direct introduction experiments.

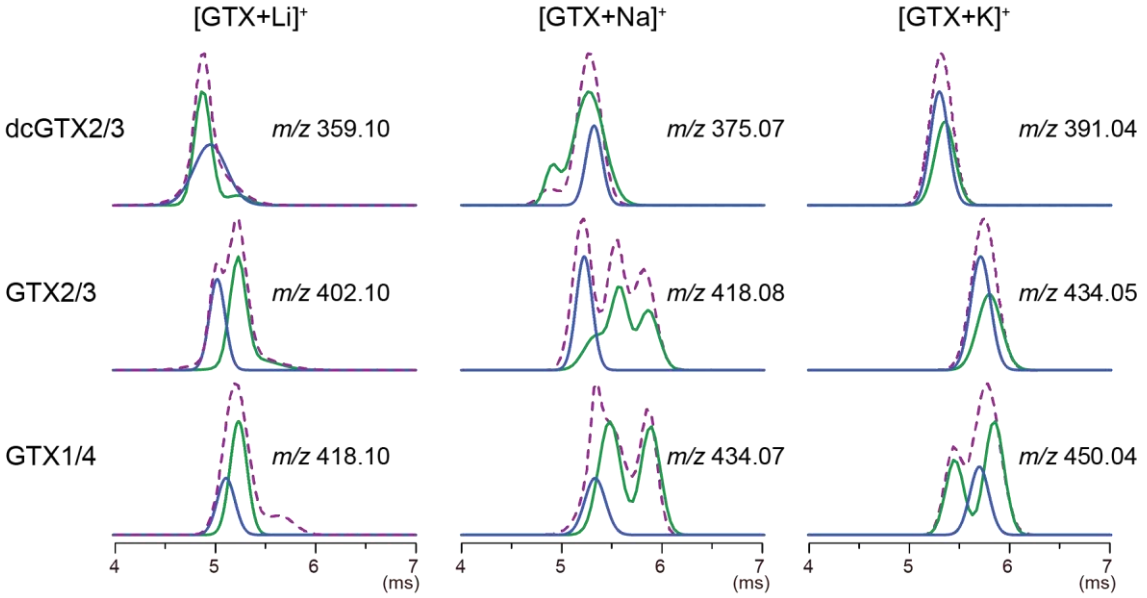

Figure S5. IM spectra observed in CO_2 in the following conditions: wave velocity 400 m s^{-1}, height wave 40 V and gas flow 90 mL min^{-1}. Green XIMS correspond to dcGTX2, GTX1 or GTX2, extracted from HILIC-IM-MS experiments and blue XIMS to dcGTX3, GTX4 or GTX3. Dashed purple XIMS correspond to the mixtures of diastereomers of dcGTX2/3, GTX1/4 or GTX2/3, extracted from direct introduction experiments.

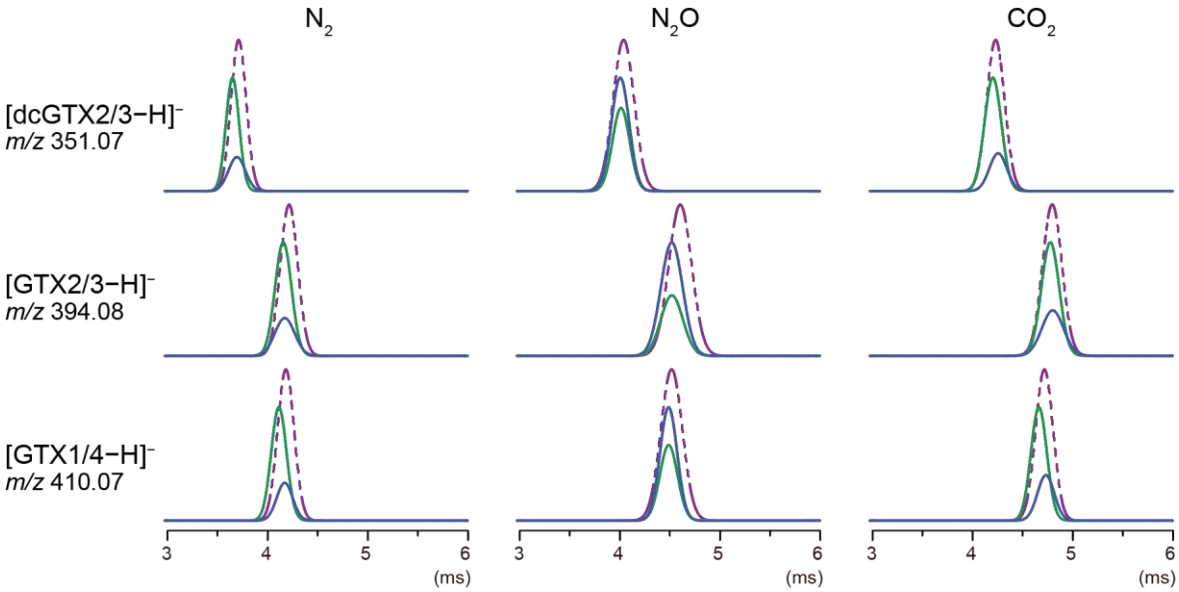

Figure S6. Extracted (HILIC)-IM-MS spectra of $[GTX-H]^-$ in N_2, N_2O and CO_2. Green XIMS correspond to dcGTX2, GTX1 or GTX2, extracted from HILIC-IM-MS experiments and blue XIMS to dcGTX3, GTX4 or GTX3. Dashed purple XIMS correspond to the mixtures of diastereomers of dcGTX2/3, GTX1/4 or GTX2/3, extracted from direct introduction experiments.

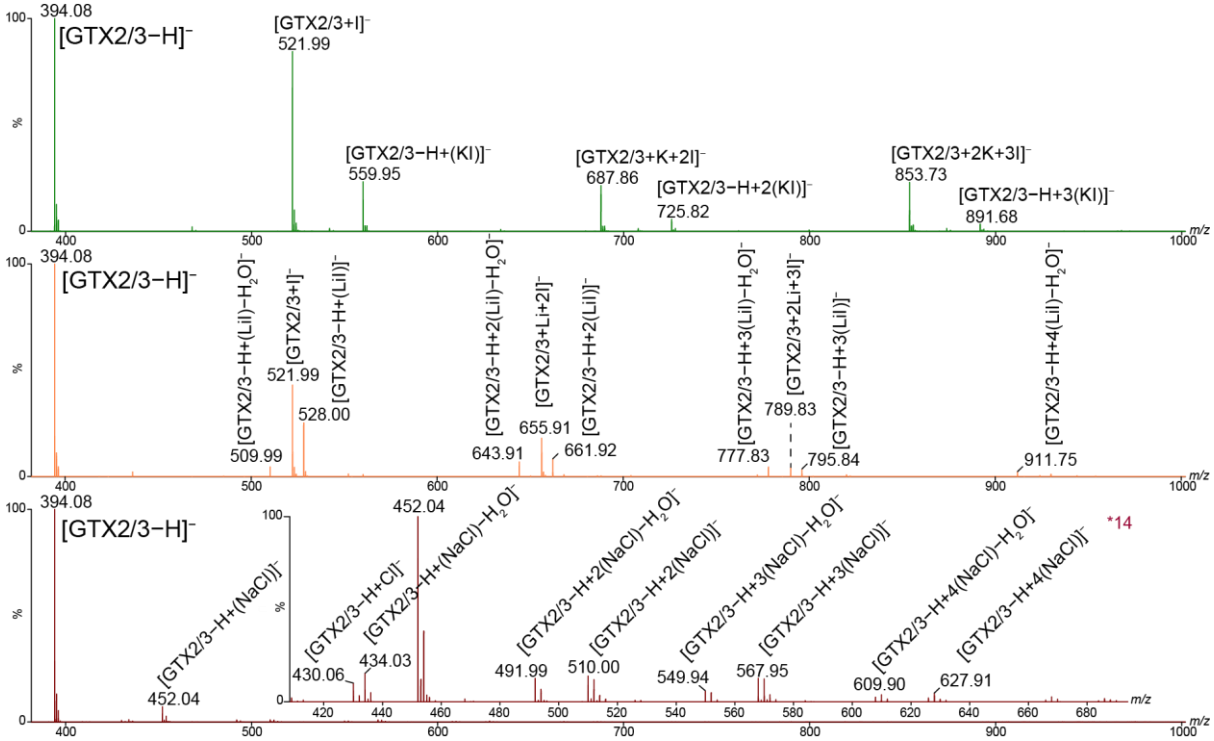

Figure S7. MS spectra of GTX2/3 extracted from LC-MS experiment with a background subtraction in the negative ionization mode.

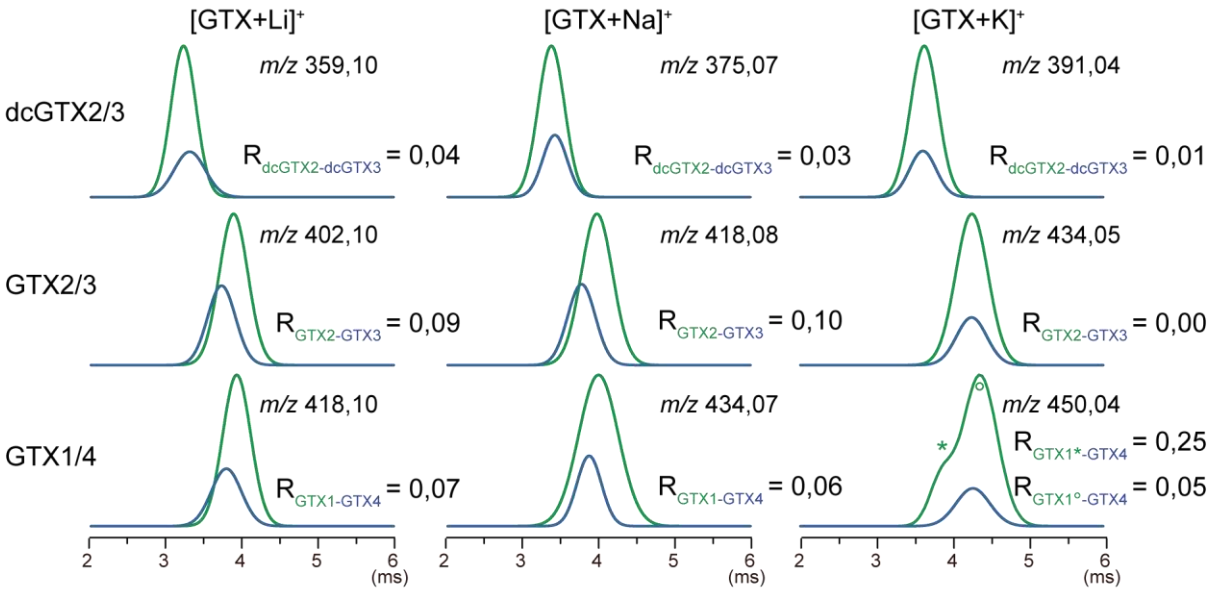

Figure S8. XIMS observed in He in the following conditions: wave velocity 600 m s^{-1}, height wave 5.5 V and gas flow 50 mL min^{-1}. Green XIMS correspond to dcGTX2, GTX1 or GTX2, extracted from HILIC-IM-MS experiments and blue XIMS to dcGTX3, GTX4 or GTX3. Dashed purple XIMS correspond to the mixtures of diastereomers of dcGTX2/3, GTX1/4 or GTX2/3, extracted from direct introduction experiments.

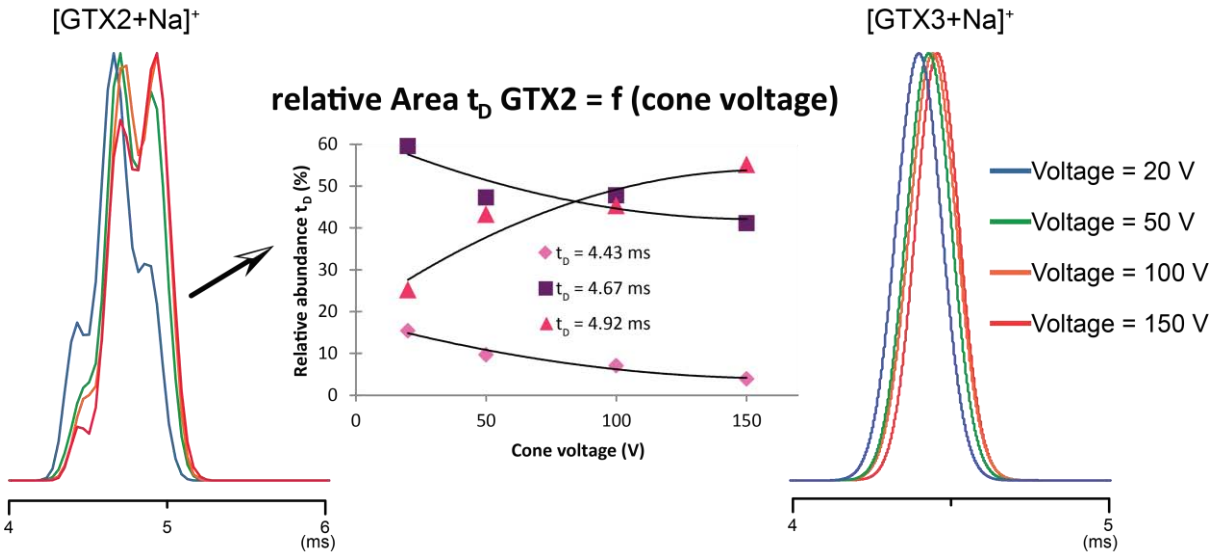

Figure S9. Normalized XIMS of $[GTX2+Na]^+$ (left) and $[GTX3+Na]^+$ (right) in function of the cone voltage. Relative areas of the different IM signal observed for $[GTX2+Na]^+$ are shown at the center in function of the cone voltage.

Figure S10. Views of selected representative DFT structures for the $[GTX2\text{-}Na]^+$ adducts, optimized at the ωB97X-D/6-311++G(d,p) level of theory. Relative energies (in kcal mol^{-1}) are given in bold and E_{ZPE} values (in Hartrees) are in parenthesis. Color code: H atoms in white, C in grey, N in blue, O in red, S in yellow, and Na in violet.

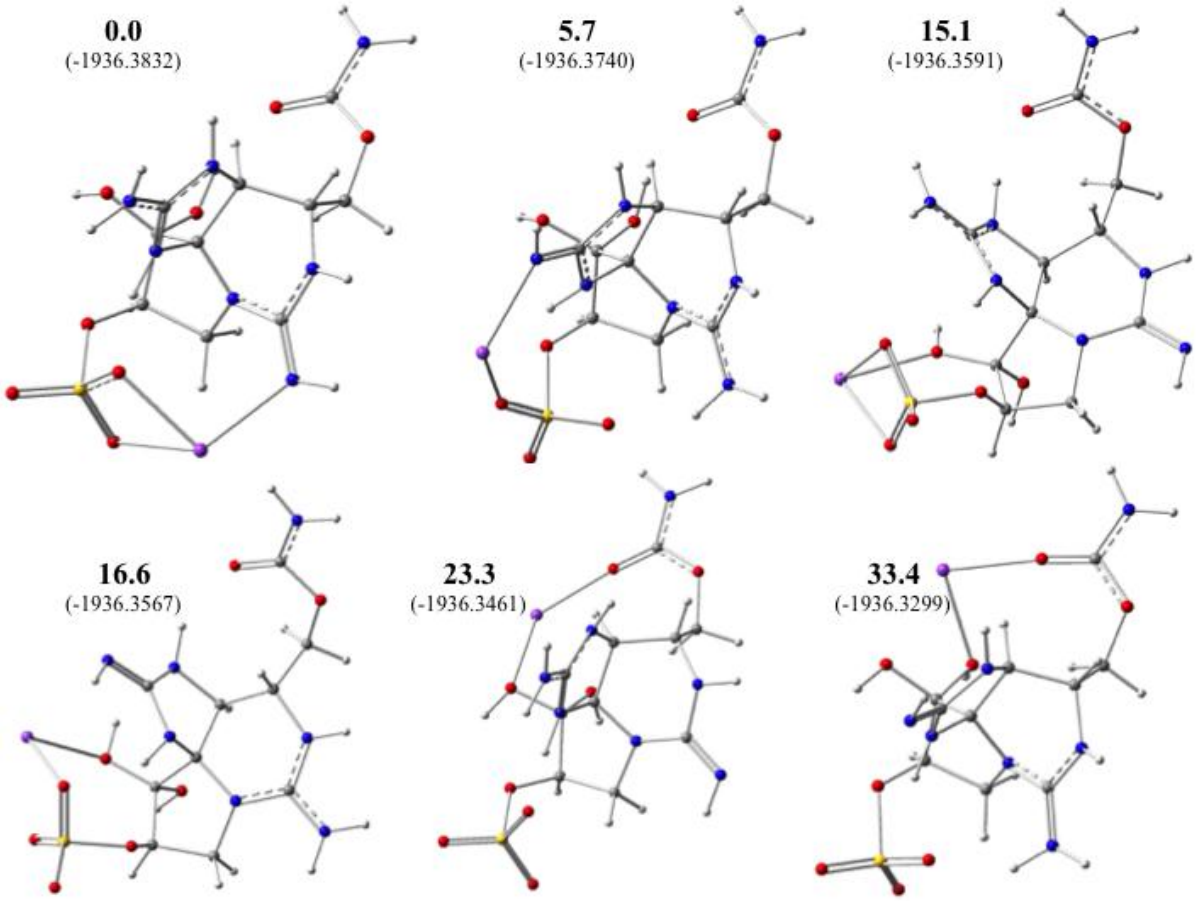

Table S1. Percentage average values of water molecule loss from alkali adducts calculated on MS peak intensity. Average calculated from n=5 analysis in MS and IM mode using different IM parameters.

	dcGTX2/3 (%)	GTX2/3 (%)	GTX1/4 (%)
Li	17 / 222	35 / 38	30 / 47
Na	46 / 141	13 / 18	8 / 22
K	2 / 4	1 / 3	1 / 3

Ratio obtained from the following calculation:

$$GTX2/3\ (\%) = \frac{[GTX2/3 + Y]^+}{[GTX2/3 + Y - H_2O]^+} \times 100$$

Table S2. t_D (ms) of the major adducts of GTXs observed in the negative ionization mode, obtained from HILIC-IM-MS experiments in N_2. The same proportions of $[GTX2/3-H+2(LiI)]^-$ were observed so they cannot be differentiated. Data in red correspond to XIMS with intensity below to 500 and then fitted with a Gaussian function, so these values are not intense enough to be considered.

	$t_{D\ dcGTX2}$	$t_{D\ dcGTX3}$	$t_{D\ GTX2}$	$t_{D\ GTX3}$	$t_{D\ GTX1}$	$t_{D\ GTX4}$
$[GTX-H+(LiI)-H_2O]^-$	4.20	4.13/4.41	4.71	4.56	-	-
$[GTX+I]^-$	4.38	4.48	4.83	4.84	4.86	4.67
$[GTX-H+(LiI)]^-$	4.29	4.24	4.88	4.88	4.94	4.82
$[GTX-H+2(LiI)-H_2O]^-$	4.67/5.00	4.68	5.29	5.10	5.20/5.44	-
$[GTX-H+2I+Li]^-$	4.96	4.91	5.45	5.44	5.50	5.14
$[GTX-H+2(LiI)]^-$	4.68/4.95	-	5.12/5.44	5.12/5.45	-	-
$[GTX-H+(NaCl)-H_2O]^-$	4.02	4.00	4.55	4.35	4.58	4.45
$[GTX-H+(NaCl)]^-$	4.09	4.03	4.53/4.73	4.51	4.61/4.83	4.60
$[GTX-H+2(NaCl)-H_2O]^-$	4.30	4.31	4.84	4.62	4.80	4.72
$[GTX-H+2(NaCl)]^-$	4.35	4.46	4.79	4.73	4.88	4.79
$[GTX+I]^-$	4.37	4.47	4.83	4.92	4.84	4.65
$[GTX-H+(KI)]^-$	4.54	4.49	5.13	4.81	5.17	4.92
$[GTX-H+2I+K]^-$	5.26	5.09	5.74	5.49	5.60	5.35
$[GTX-H+2(KI)]^-$	5.07	-	5.64	5.45	5.69	-

Table S3. Experimental CCS values obtained for IMS experiments obtained with N_2 as drift gas using either polyalanine He or N_2 database for calibration. Calculated CCS were obtained using different MOBCAL version described below. Values between parentheses correspond to the standard deviation of MOBCAL carried out on the most stable structures for a given compound ($E_{ZPE} < 6$ kcal mol^{-1}).

Toxin	Generated structures	CCS_{exp} (Å²)		Averaged CCS_{calc} (Å²)	
		He	N_2	He	N_2
$[GTX2+Li]^+$	1	121	189	110.4	190.5
$[GTX3+Li]^+$	5	118	185	112.7 (1.4)	195.5 (2.7)
$[GTX2+Na]^+$	2	122/127/131	189/195/200	111.3	191.2
$[GTX3+Na]^+$	5	121	188	114.5 (1.8)	197.9 (3.1)
$[GTX2+K]^+$	2	129	198	113.8	195.4
$[GTX3+K]^+$	4	128	197	116.3 (1.9)	199.9 (2.8)

Trajectory method algorithm of Martin Jarrold group was used with modified Lennard-Jones parameters preconized for He calculation to determine CCS_{calc} in He [19, 40]. The N_2 version of MOBCAL was used to calculate CCS_{calc} in N_2 as it takes into account the charge induced-dipole interaction between the ion and the drift gas [38].

200000 points were generated for each calculation (itn = 20, inp = 20 and imp = 500).

In both versions of MOBCAL, inversion of CCS order for isomer couples were observed between calculated and experimental CCS values (*i.e.* $CCS_{calc}[GTX3+Li]^+ > CCS_{calc}[GTX2+Li]^+$ whereas $CCS_{exp}[GTX3+Li]^+ < CCS_{exp}[GTX2+Li]^+$).

It should be pointed out that even if inversion is observed, the N_2 version of MOBCAL showed less deviation between CCS_{exp} and CCS_{calc}: deviation from 1 to 5 % for N_2 CCS values and from 5 to 14 % for He values.